PCCP

View Online
Dynamic Article Links

Cite this: DOI: 10.1039/c1cp20352e

www.rsc.org/pccp

PAPER

Modeling and characterization of extremely thin absorber (eta) solar cells based on ZnO nanowires†

Iván Mora-Seró,*[a] Sixto Giménez,[a] Francisco Fabregat-Santiago,[a] Eneko Azaceta,[b] Ramón Tena-Zaera*[b] and Juan Bisquert[a]

Received 6th December 2010, Accepted 9th February 2011
DOI: 10.1039/c1cp20352e

Extremely thin absorber (eta)-solar cells based on ZnO nanowires sensitized with a thin layer of CdSe have been prepared, using CuSCN as hole transporting material. Samples with significantly different photovoltaic performance have been analyzed and a general model of their behavior was obtained. We have used impedance spectroscopy to model the device discriminating the series resistance, the role of the hole conducting material CuSCN, and the interface process. Correlating the impedance analysis with the microstructural properties of the solar cell interfaces, a good description of the solar cell performance is obtained. The use of thick CdSe layers leads to high recombination resistances, increasing the open circuit voltage of the devices. However, there is an increase of the internal recombination in thick light absorbing layers that also inhibit a good penetration of CuSCN, reducing the photocurrent. The model will play an important role on the optimization of these devices. This analysis could have important implications for the modeling and optimization of all-solid devices using a sensitizing configuration.

1. Introduction

Semiconductor sensitized solar cells have attracted a growing interest in the last few years.[1–7] Among them, extremely thin absorber (eta)-solar cells[4,8] appear as an attractive option due to their full solid state character and the consequent robustness. These devices are based on a thin (few tens of nm) layer of a light absorber semiconductor sandwiched between both solid electron and hole conductors.

Since the eta-solar cell concept was proposed in 2000 by Konenkamp *et al.*,[8] continuous and progressive improvements have been achieved. After some interesting reports on the integration of different materials in the eta-solar cell architecture,[9] Lévy-Clément *et al.* demonstrated in 2005 the experimental feasibility of the concept for ZnO/CdSe/CuSCN solar cells (efficiency, $\eta \sim 2.3\%$ under 360 Wm^{-2} illumination) based on ZnO nanowire arrays.[4] In 2008, Dittrich's group also used ZnO nanowire arrays as building blocks for ZnO/In_2S_3/CuSCN eta-solar devices, reaching conversion efficiencies up to 3.4%.[10] Similar efficiencies were also reported in the last two years for devices based on nanocrystalline TiO_2 using Sb_2S_3 as a light absorber, keeping CuSCN as a hole collector.[11–13] Organic compounds such as spiro-OmeTAD[14] and P3HT[3] have been recently used as alternative hole conductors, reaching conversion efficiencies above 5% for the latter.[3] Krunks *et al.* have also reported an efficiency of 4.2% for ZnO/In_2S_3/$CuInS_2$ nanowire array based eta-solar cell.[15]

The fundamentals of eta-solar cells are analogous to those of dye sensitized solar cells (DSC).[16] Photogenerated carriers in molecular dyes (DSCs) or semiconductor extremely thin light absorber layer (eta-solar cell) are quickly injected into two different transport media, see Fig. 1. Carrier separation significantly slows down the recombination process. This fact allows a significant relaxation of the quality required for the materials with the concomitant reduction of the production costs. Therefore, this technology constitutes an extremely attractive alternative to develop low cost photovoltaic devices. In order to increase the light harvesting capabilities of DSC, nanostructured architectures are required to increase the amount of light absorbing materials. Since the extinction coefficient of semiconductors is higher compared to metallorganic dyes,[17] the increase of the effective area of the nanostructured electrode does not need to be so high compared to DSCs. For this purpose, one dimensional structures as ZnO nanowire (NWs) arrays offer an effective solution. Single-crystal ZnO NWs with excellent transport properties can be easily grown by low cost techniques, such as electrodeposition.[4,18,19] Indeed, ZnO NW arrays have played an important role in the development of eta-solar cells.[4,10,15]

The evolution of the eta-solar cell efficiency during the last five years is clear evidence of the high potential of this

[a] *Grup de dispositius Fotovoltaics i Optoelectrònics, Departament de Física, Universitat Jaume I, 12071 Castelló, Spain. E-mail: sero@fca.uji.es*
[b] *CIDETEC-ik4 (Centro de Tecnologías Electroquímicas), Parque Tecnológico de San Sebastián, Paseo Miramón, 196, 20009 Donostia - San Sebastián, Spain. E-mail: rtena@cidetec.es*
† Electronic supplementary information (ESI) available. See DOI: 10.1039/c1cp20352e

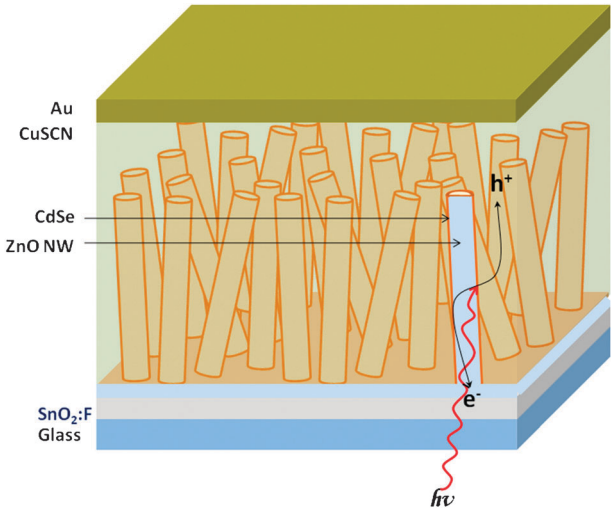

Fig. 1 Scheme of the analyzed eta-solar cell. Light generates electron-hole pairs in the semiconductor absorber (CdSe), the electron is injected into a ZnO nanowire employed as electron conductor, and it is transported in this medium to the transparent conductive oxide $SnO_2:F$ used as collecting substrate and light window. The hole is injected into the CuSCN. Finally the hole is transported to the counter electrode (Au).

technology. However, further improvements related to the conversion efficiency are still necessary for it to become a competitive electricity production technology. Although there are a few theoretical models[20] and fundamental experimental studies about the electrical transport mechanisms,[21] to our knowledge, there are no reports which correlate models with experimental data. In this framework, impedance spectroscopy (IS) appears to be a powerful technique. IS has been used successfully to characterize ZnO NW arrays[18,22,23] and this characterization technique has proved essential to enhance the understanding and the improvement in cell performance of DSCs.[24]

In this report, we analyze ZnO/CdSe/CuSCN nanowire array based eta-solar cells with significant differences in their photovoltaic parameters (*i.e.* short circuit current, open circuit voltage, fill factor and conversion efficiency) by IS. A model was developed to fit the experimental IS spectra. On the other hand, the cross sections of the devices were analyzed by scanning electron microscopy (SEM). The origin of the differences observed for the photovoltaic parameters are discussed by correlating the electrical and microstructural properties of the interfaces of the device characterized through IS and SEM, respectively. The present analysis could have important implications for the modeling and optimization of sensitized (semiconductor or dye) solid state devices.

2. Experimental

Sample fabrication

The eta-solar cell fabrication consisted of four different steps: (a) electrodeposition of ZnO nanowire arrays, (b) electrodeposition of the CdSe coating on the ZnO nanowire arrays, (c) filling the ZnO/CdSe nanostructure with CuSCN and (d) thermal evaporation of a gold layer.

(a) ZnO NW arrays were electrodeposited from the reduction of dissolved molecular oxygen in zinc chloride solutions.[18,19] The electrodeposition experiment was performed in a three-electrode electrochemical setup using an EC-Laboratory MPG Biologic Multirespotentiostat. The cathode was a commercial conducting glass/$SnO_2:F$ (TEC15,Hartford Glass Co) substrate, FTO, which was previously covered by a thin compact ZnO sprayed layer, ZnO_{sp},[25] a Pt spiral wire as the anode and a saturated calomel electrode (SCE) as the reference electrode. The electrolyte was a 5×10^{-4} M $ZnCl_2$ (>98.0%), 2 M KCl (>99.5%) ultrapure aqueous solution, saturated by bubbling oxygen. The deposition was performed at 70 °C at constant potential ($V = -1$ V *vs.* SCE). The length of the ZnO NWs, ZnO_{NW}, was varied by modifying the charge density passed during the electrodeposition.

(b) The CdSe coating layer was electrodeposited, from an aqueous selenosulfate solution,[26,27] in a two-electrode electrochemical cell with the glass/$SnO_2:F/ZnO_{sp}/ZnO_{NW}$ array as the cathode and a Pt spiral wire as the counter electrode. The charge density passed during CdSe electrodeposition was held constant at 0.25 C cm^{-2} for all samples. The obtained ZnO/CdSe core-shell nanowire arrays were annealed in air at 350 °C for 1 h.

(c) The CuSCN layer was deposited, from a saturated solution of CuSCN in propylsulfide,[28] on pre-heated ~100 °C glass/$SnO_2:F/ZnO_{sp}/ZnO_{NW}$/CdSe samples. The amount of solution used in the CuSCN deposition process was 0.1 mL cm^{-2}.

(d) A gold layer was deposited on the CuSCN layer by using a NANO38 thermal evaporator.

After this process, a complete eta-solar cell device is obtained, see Fig. 1. Blank samples without the CdSe light absorbing layer were also prepared following exactly the same procedure used in eta-solar cell manufacturing but without step b. In addition, flat samples of glass/$SnO_2:F$/CuSCN/Au have been fabricated by applying steps c and d on FTO substrates.

Sample characterization

The microstructural features of the device cross sections were analyzed using a JEOL-JSM-7000F field emission scanning electron microscope (FE-SEM). The current–voltage characteristics of the cells were measured using a xenon arc lamp simulator (Sun 2000, ABET Tehnologies) with an AM 1.5 G spectral filter, and the intensity was adjusted to provide 1 sun (100 mW cm^{-2}) using a calibrated silicon solar cell. IS measurements were obtained using a FRA equipped PGSTAT-30 from Autolab. The solar cells have been characterized under dark and illuminated conditions and the blank samples under dark conditions. For IS characterization, the cells were illuminated using a white LED system calibrated to 1 sun intensity (100 mW cm^{-2}). IS measurements were carried out at forward bias, applying a 20 mV AC sinusoidal signal over the constant applied bias with the frequency ranging between 400 kHz and 0.1 Hz. In order to verify the stability of the cells during IS measurements, J–V curves have been performed before and after IS. No significant variation has been observed indicating a good stability during the measurement.

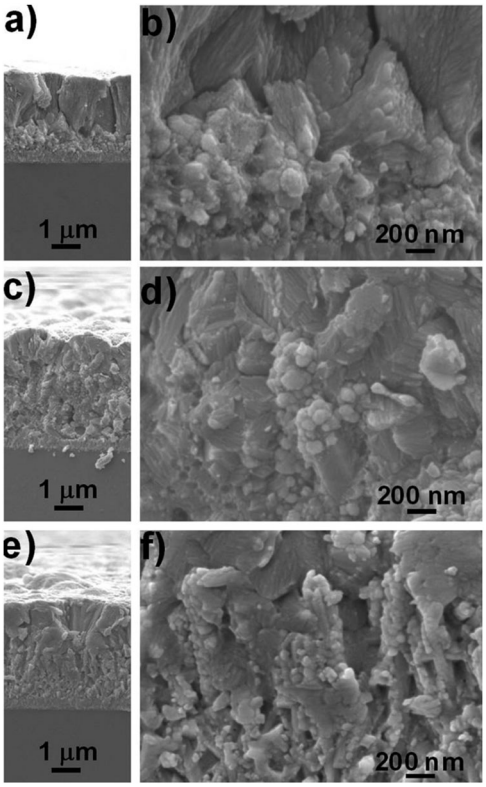

Fig. 2 SEM micrographs of cells 10 (a, b), 18 (c, d) and 19 (e, f). Left side: Cross section of the full device. Right side: High magnification view of the ZnO/CdSe/CuSCN interface.

It is worth mentioning that very good reproducibility was checked, by using different characterization techniques, for ZnO/CdSe samples.[27] However, the current–voltage characteristics of ZnO/CdSe/CuSCN eta-solar cells exhibit significant dispersion. The latter suggests some crucial reproducibility problems in the CuSCN deposition step. In order to gain a further insight into this matter, the cross section of different ZnO/CdSe/CuSCN eta-solar was analyzed by SEM. A correlation between CuSCN penetration into the ZnO/CdSe nanowire structure and photocurrent values was generally observed—poor penetration results in relatively low photocurrents and high photovoltages.

Three eta-solar cells, thereafter labeled as 10, 18 and 19, with different architectural features (Fig. 2), showing also significant differences in the photovoltaic performance (Fig. 3), were then selected for IS studies. Table 1 summarizes the microstructural features of the analyzed eta-solar cells. They exhibit different ZnO NW geometry although all of them contain the same total amount of CdSe and CuSCN. Consequently, the local thickness of the CdSe and CuSCN overlayer increases as $10 < 18 < 19$.

Table 2 displays the photovoltaic parameters, extracted from the *I–V* curves (Fig. 2), of the eta-solar cells. Significant differences among the samples can be appreciated with a characteristic trend: a reduction of the cell photocurrent, j_{sc}, as the photovoltage, V_{oc}, increases. The different photovoltaic performance (beyond their conversion efficiency) makes the selected samples a good scenario to develop and test a general model for eta-solar cell characterization.

3. Modeling aspects

The eta-solar cells are conceptually very similar to the dye sensitized solar cells. The operation of both types of cells is characterized by the quick extraction of photogenerated carriers into two different transporting media, as previously discussed.

There are well established models for the characterization of sensitized solar cells using molecular dyes[24] or semiconductor quantum dots[1,29] as light sensitizers and TiO_2 nanoparticles network as electron transporter material. In order to model the impedance of porous materials, these models include extended elements based on the concept of a transmission line,[30] which is widely accepted to model the electron transport and recombination in different porous systems ranging from solar cells to supercapacitors. A more detailed description of transmission lines and their applicability can be found elsewhere.[31]

Therefore, the general model for DSC, see Fig. 4(a), is an excellent starting point for obtaining an eta-solar cell model including the specific characteristics of the analyzed cell. The equivalent circuit on Fig. 4(a) reflects the physical processes of carrier transport, charge transfer and recombination, which take place in the DSC device. C_μ ($= c_\mu \times L$, where L is the TiO_2 layer thickness) is the chemical capacitance[32] of the TiO_2 semiconductor. R_{tr} ($= r_{tr} \times L$) is the electron transport resistance in the TiO_2, directly related to the electron conductivity in TiO_2 as $\sigma_n = L/R_{tr} \times S$, where S is the area. R_r ($= r_r \times L$) is the recombination resistance, a charge-transfer resistance related to recombination of electrons at the TiO_2/hole conductor interface. R_s is a series resistance accounting for the transport resistance of the transparent conducting oxide and the connection setup. Z_d is the impedance assigned to the hole transporter media. R_{CE} represents the charge transfer resistance at the counter electrode/electrolyte interface. C_{CE} is the interfacial capacitance at the counter electrode/electrolyte interface.

In the particular case of the analyzed eta-solar cells, electrodeposited ZnO nanowires present a high intrinsic *n* doping[22,23] and single-crystal character,[33] indicating good transport characteristics. This fact suggests that a very low R_{tr} should be expected for electrodeposited ZnO NWs and the electron transporting media can be modeled as a short circuit. Consequently, the transmission line in the equivalent circuit for DSC in Fig. 4(a) is reduced to a simple *R–C* circuit, see Fig. 4(b), taking into account the recombination resistance and the capacitance of the system, C. The latter, in the case of ZnO NWs, will be the NW depletion capacitance within a certain voltage range, as we have demonstrated.[22,23]

$$C = \frac{2\pi\varepsilon LDS}{\ln\left(\frac{R}{x}\right)} \quad (1)$$

where $\varepsilon = \varepsilon_r\varepsilon_0$, $\varepsilon_r = 10$ is the dielectric constant of the ZnO nanowires and ε_0 is the dielectric constant of vacuum. L, R and D are the NW length, radius and the surface density of NWs in the array, respectively. S is the total flat surface. Finally x is the thickness of the depletion region, which is related to the potential drop across the semiconductor space-charge region, V_{sc}:

$$V_{sc} = \frac{qN_D}{2\varepsilon}\left[\frac{1}{2}(x^2 - R^2) + x^2\ln\left(\frac{R}{x}\right)\right] \quad (2)$$

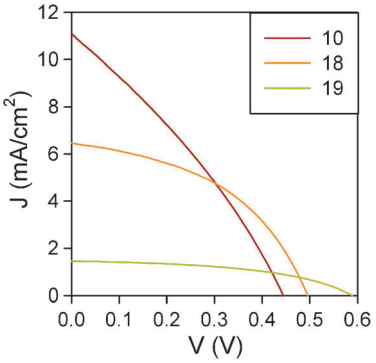

Fig. 3 *J–V* curves of analyzed eta-solar cell under 1 sun illumination (AM 1.5 G).

where q is the positive elementary charge and N_D is the donor density.

Additionally, since the contact between CuSCN and Au exhibits good electrical characteristics and consequently low R_{CE}, the R_{CE}–C_{CE} circuit can be neglected, see Fig. 4(b). The determination of Z_d for the hole conductor material and how it can be identified from the IS pattern is a particularly challenging issue. Regarding DSC with a liquid electrolyte, Z_d is identified from the IS pattern as an arc appearing at the low frequency region at high forward bias.[24] When the solid hole conductor OMeTAD is employed, a characteristic arc at high frequencies is observed in the impedance spectra.[34] To the best of our knowledge, there are no previous reports concerning the characteristic impedance of CuSCN. In order to determine its behavior and pattern, flat samples of CuSCN, sandwiched between two contacts, have been prepared; see Fig. 5(a). An example of the Nyquist plots obtained for CuSCN flat samples is plotted in Fig. 5(b). CuSCN samples present the characteristic pattern of a Warburg element, with a straight line closing in an arc,[35] produced by carrier diffusion process. It is worth noting that the arc appears at high frequencies as for OMeTAD transporter. This is due to the faster diffusion compared to the liquid electrolyte.

4. Results and discussion

Taking into account these previous considerations, eta-solar cells have been analyzed by IS under dark and illumination conditions, considering the equivalent circuit plotted in Fig. 4(b). Warburg element is used as Z_d, and a constant phase element (CPE) instead of a capacitor is employed to take into account non-ideal behavior. CPE impedance is defined as: $Z_{CPE} = 1/Q(i\omega)^n$, where $i = \sqrt{-1}$, ω is the angular frequency, Q is a magnitude with $F \times s^n$ units and n an exponent with values between 0 (ideal resistance) and 1 (ideal capacitance). The capacitance has been obtained considering that for a R-CPE parallel association the capacitance is calculated as[36]: $C = (RQ)^n/R$.

Fig. 6(a) and (b) display an example of the Nyquist plots obtained from the EIS characterization of the complete eta-solar cells. At the low frequency region of the spectra, an arc corresponding to the R_r–CPE in the equivalent circuit 4(b) is observed. At the high frequency region, the straight line characteristic of the Warburg impedance is clearly observed in the magnified plot, Fig. 6(b). Excellent agreement between the experimental data and the fitting parameters using the equivalent circuit described in Fig. 4(b) has been achieved; see Fig. 6(a) and (b).

Table 2 Photovoltaic properties of the manufactured eta-solar cells, photocurrent j_{sc}, open circuit voltage V_{oc}, fill factor FF, and efficiency η, for the different samples tested under standard conditions (100 mW cm^{-2} AM 1.5G)

Sample	V_{oc} (V)	j_{sc} (mA cm^{-2})	FF	η (%)
10	0.447	11.1	0.31	1.52
18	0.497	6.48	0.45	1.45
19	0.593	1.45	0.48	0.41

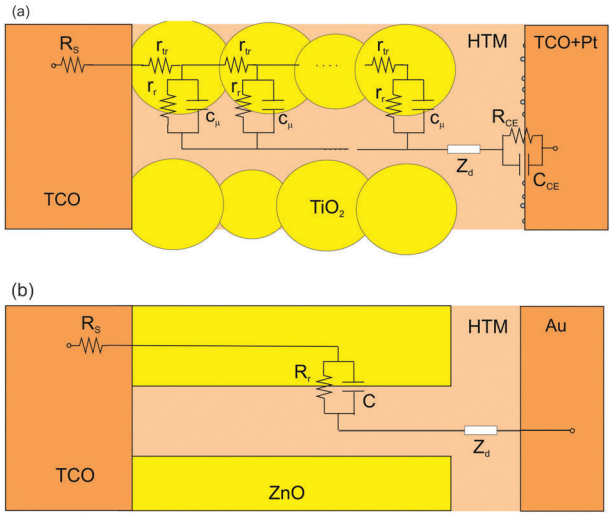

Fig. 4 (a) Equivalent circuit employed in DSCs,[24] (b) equivalent circuit employed to fit the IS data obtained for eta-solar cells based on ZnO NWs.

Table 1 Average nominal values of ZnO nanowire length, L, NW diameter, R, and NW density, D, and thickness of the overlayer of CuSCN, L_{CuSCN}, on top of ZnO NWs array, obtained from SEM micrographs. Total surface of the NW array per square centimetre of substrate surface obtained from the nominal values, S_n. Donor density obtained from the fit of eqn (1) and (2) and using S_n as the surface of NW array, N_{D-n}. Total surface of the NW array per square centimetre of substrate surface obtained from the fit of eqn (1) and (2) leaving the surface of NW array as a fit parameter, S_{fit}. Donor density obtained from the fit of eqn (1) and (2) and leaving S_{fit} as a fit parameter, $N_{D\text{-fit}}$

Sample	L (nm)	R (nm)	D ($10^9 \times$ cm^{-2})	L_{CuSCN} (nm)	S_n (cm^2)	S_{fit} (cm^2)	N_{D-n} ($10^{17} \times$ cm^{-3})	$N_{D\text{-fit}}$ ($10^{17} \times$ cm^{-3})
10	2500	140	2	650	45.2	—	0.8	—
18	1700	90	3	1800	29.6	9.86	2.0	1.0
19	500	90	3	2000	9.25	3.1	3.3	1.8
B3	1700	90	3	1000	29.6	—	—	—
B4	1700	90	3	2000	29.6	—	—	—

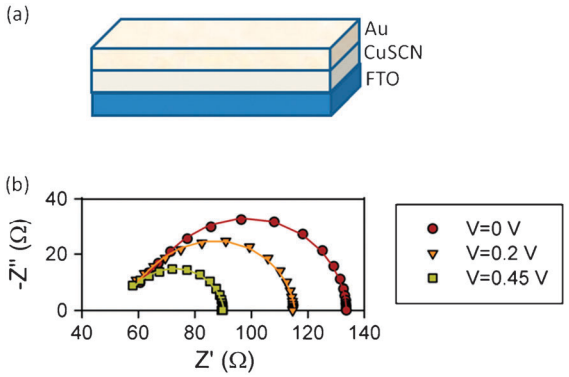

Fig. 5 (a) Scheme of the CuSCN thin layer characterized by impedance spectroscopy. (b) Impedance spectroscopy measurement of CuSCN sample (symbols) at different applied forward bias, V, under dark conditions. Solid lines correspond to the fit using a Warburg element in series with a series resistance as equivalent circuit.

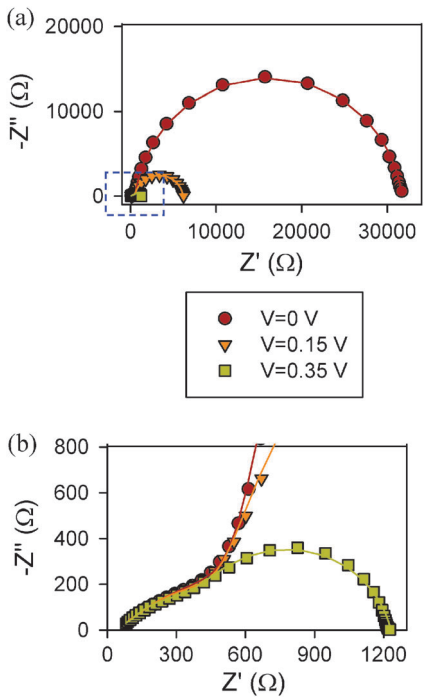

Fig. 6 (a) Impedance spectroscopy measurement of eta-solar cell sample 10 (symbols) at different applied forward bias, V, under dark conditions. Solid lines correspond to the fit using the equivalent circuit shown in Fig. 3b. (b) Magnification of the dashed rectangular area in graph (a), where the Warburg pattern can be clearly identified from the IS spectra.

The extraordinary power of IS as device characterization technique lays in the ability to discriminate among different processes. This fact allows an individual study for each process. In our case, two processes can be clearly distinguished: hole transport in the CuSCN layer (Warburg) and interfacial process (R_r–CPE) at the ZnO/CdSe/CuSCN junction.

Focusing on the first process, hole transport in the CuSCN layer, the fitting process permits extracting the parameters of the Warburg element from its impedance, Z_W:

$$Z_W = R_W \times \tanh((i\omega W)^p)/(i\omega W)^p \qquad (3)$$

where R_W is the transport resistance of the system, p is a parameter with 0.5 value in the case of diffusion and W is related to the diffusion coefficient, D, as $W = L^2/D$, where L is the effective diffusion length of the system. Considering the length of CuSCN, L, as the sum of ZnO NW length plus the CuSCN overlayer thickness, both hole conductivity, σ_h, and hole diffusion coefficient, D_h, in CuSCN have been obtained, see Fig. 7.

The conductivity obtained under dark conditions, Fig. 7(a), is very similar for either the eta-solar cells or the blank samples, except for sample 18, with lower conductivity values. Under illumination conditions, Fig. 7(b), the conductivity increases for samples 10 and 18, particularly at low applied voltages. This increase is due to the higher hole density in CuSCN under illumination as a consequence of hole injection from the CdSe light absorbing layer. The difference in hole density between dark and illuminated conditions is more pronounced at low applied voltages. This explains the higher increase of conductivity observed in this region. As expected, the highest hole injection for sample 10 under illumination (producing the highest conductivity) correlates to the highest measured photocurrent (11.1 mA cm^{-2}). The lowest hole injection (lowest conductivity) is obtained for cell 19 and also correlates to the lowest measured photocurrent (1.45 mA cm^{-2}). The low hole injection for cell 19 is the reason why the conductivity does not vary significantly between the dark and illuminated conditions, see Fig. 7(a) and (b).

On the other hand, similar diffusion coefficients have been obtained for all the samples, with the only exception being

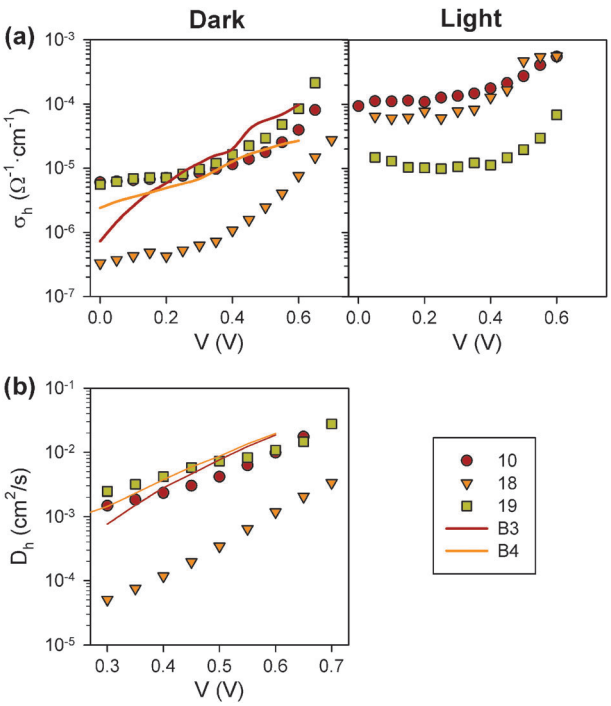

Fig. 7 IS characterization of eta-solar cells. (a) Hole conductivity, σ_h, of the CuSCN layer under dark (left) and under 1 sun illumination (right) conditions. (b) Hole diffusion coefficient in CuSCN, D_h, under dark conditions. The solid lines correspond to the blank samples (B3 and B4) without semiconductor absorbing layer and different CuSCN thickness as reported in Table 2.

sample 18 (Fig. 7(b)). Basically, the transport properties of the CuSCN layer remain similar for all the samples independently of the ZnO NW geometry and the presence of the CdSe absorbing layer. Consequently, we cannot identify this process as the origin of the different cell performances observed in Fig. 3 and Table 2. Under illumination conditions, the working conditions of the cell, σ_h, for cell 18 lies between the conductivity of cells 10 and 19 as it is expected from its photocurrent, see Table 2 and Fig. 7(b).

The interfacial process at the ZnO/CdSe/CuSCN interface is characterized by an R_r–CPE circuit. Recombination resistance and capacitance can be obtained from the fitting of the impedance spectra using the equivalent circuit in Fig. 4(b). The obtained values for the different cells are plotted in Fig. 8. Analyzing the recombination resistance under dark conditions, a clear trend is visible. R_r decreases as the applied voltage increases for all the samples, cells and blanks, due to the increase of electron density with voltage, see Fig. 8(a). In addition, the slope is also similar for all cases, although full cells exhibit higher recombination resistance compared to blank samples. This fact clearly indicates that the CdSe light absorbing layer acts as blocking layer slowing down the recombination process between photoinjected electrons in ZnO and photoinjected holes in CuSCN. Comparing the cells, R_r increases as 10 < 18 < 19, following exactly the same trend

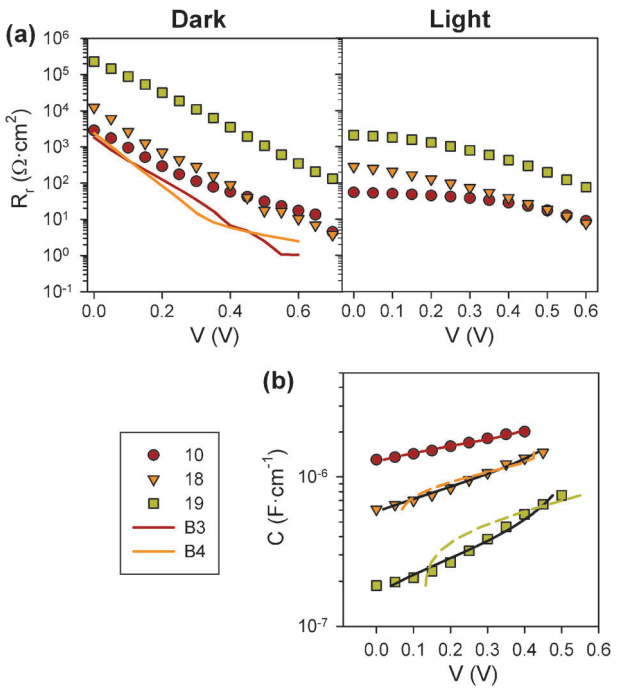

Fig. 8 Impedance spectroscopy characterization of eta-solar cells. Behavior of the recombination resistance and capacitance. (a) Recombination resistance, R_r, under dark (left) and illuminated (right) conditions. Solid lines correspond to two blank samples, as indicated in the legend, with no semiconductor absorbing layer and different CuSCN thickness. (b) Capacitance obtained from IS measurements (symbols). Dashed lines correspond to the fitting of capacitance taking into account the nominal density of ZnO NWs. Black solid lines correspond to the fitting of capacitance leaving the density of ZnO nanowires as a free parameter in the fitting process.

observed for the open circuit voltage, see Table 2. The cause of lower V_{oc} for cells 10 and 18 compared to cell 19 is due to an increase of recombination. The presence of the absorbing layer and the thickness of this layer reduce the recombination process. This trend also applies under light conditions, see Fig. 8(a). An increase of recombination (lower R_r), particularly at lower applied bias, is observed. This is expected from the increase of electron density in the ZnO NWs due to the injection of photogenerated electrons. The same behavior has been observed for quantum dot sensitized solar cells with quantum dots grown by successive ionic layer adsorption and reaction (SILAR). R_r increases with the number of SILAR cycles.[1]

Concerning the capacitance, see Fig. 8(b), its absolute value shows an opposite behavior compared to the recombination resistance, obtaining higher capacitance values for the cells with higher photocurrents. According to the model summarized in eqn (1) and (2) the capacitance should be related with the depletion capacitance of ZnO NWs at low applied forward bias.[22,23] We have fitted the obtained capacitance, using eqn (1) and (2). The result of the fitting using the nominal surface of the ZnO NW array, obtained from SEM micrographs, is displayed in Fig. 8(b) as dashed lines. The obtained donor density, N_{D-n}, see Table 1, is in good agreement those previously reported previous reports for ZnO NW arrays electrodeposited under the same conditions and annealed in air.[23]

There is a good agreement between the experimental data and the fitting for cell 10, the cell with the highest capacitance and highest photocurrent. However, when the absolute value of capacitance decreases, there is no good agreement between the experimental data and the fitted values. This discrepancy is particularly visible for cell 19, the cell with the lowest capacitance. For this cell, a rapid decrease of capacitance is observed for the fit curve at voltage values between 0.1 and 0.2 V. In our model, this decrease originates from a complete depletion of the NW,[23] but this is not observed in the experimental data. Given the large effective area of the ZnO NW array, see Table 1, the experimental capacitances obtained are lower compared to those expected for samples with the donor density commonly observed ($\sim 10^{17}$ cm^{-3}). For those donor densities and effective surfaces, see Table 1, a complete depletion of ZnO NW should take place, which is not observed experimentally. However, the expected capacitance would be lower if the effective surface of ZnO NW array is lower. A second fit rendering the total surface of the array as a free parameter (or more precisely: leaving the NW density as a free parameter) provides an excellent agreement between experimental data and fit curves, see solid black lines in Fig. 8(b). Poor penetration of the hole transporter material into the NW structure could explain this reduction in the effective surface of the NW array. A poor penetration of CuSCN in the nanostructure renders part of the CdSe light absorbing layer without hole extracting contact. Since both photogenerated carriers cannot be quickly injected into the transporter media, the key-point for eta-solar cells operation, recombination in the absorbing layer, becomes the dominant process.[2,27] Two consequences could be extracted from the bad interpenetration of CuSCN: (i) The active surface of ZnO is reduced compared to the nominal surface; and most important (ii) a bad interpenetration reduces

the obtained photocurrent as photogenerated carriers recombine before they are injected into the transporting media. In this sense, the capacitance extracted from IS could provide qualitative information of the microstructural features of the device interfaces. The thickness of the CdSe layer increases for the analyzed cells as 10 < 18 < 19, reducing the width of the channels for CuSCN penetration; consequently the photocurrent also decreases in the same fashion, see Table 2.

In SEM micrographs (Fig. 2), it is observed that the NW architecture is almost lost in device 19, since the CdSe shell is thick enough to produce the coalescence of neighboring nanowires, leading to an almost planar-like architecture. The concomitant decrease in the junction surface appears to be the main cause for the observed increase of the recombination resistance and consequently the highest V_{oc}. Furthermore, the relatively thick CdSe may also be beneficial for increasing the recombination resistance. The cross section micrographs of the device 18 shows some uncovered ZnO/CdSe nanowires and also some voids (see Supporting Information, Fig. S1†), revealing uncompleted filling of the ZnO/CdSe nanostructure with CuSCN. This is not the case in device 10, where no voids were observed. Furthermore, clear "fingerprints" in the CuSCN from nanowires and even from CdSe crystals were clearly detected in the micrographs of device 10 (Fig. S2, Supporting Information†), indicating a very good CuSCN penetration and the consequent fully interpenetrating ZnO/CdSe/CuSCN interface. This seems to be the main cause of the highest capacitance and therefore the highest j_{sc} in device 10, as has been previously discussed. However, the largest interface area, and the presence of ZnO not totally covered with CdSe (Fig. S2, Supporting Information†), seems to decrease the recombination resistance, leading to the lowest V_{oc}.

5. Conclusions

A general model for eta-solar cells based on ZnO NW arrays has been developed. The model allows distinguishing the different processes taking place in these devices. Consequently, it is possible to separately analyze each one, by IS measurements. Series resistance, hole transport, and interfacial processes have been identified and separately analyzed for samples with significantly different solar cell performance. The hole transport process is similar for all the analyzed samples. In contrast, a different behavior is obtained for recombination resistance and capacitance. Higher recombination resistance, originating from thick CdSe layer, leads to higher photovoltages. However, a thick CdSe layer also increases the internal recombination within the light absorbing layer reducing the photocurrent and inhibiting a good CuSCN penetration. This fact is clearly reflected by a reduction in the measured capacitance. Consequently, a balance between photocurrent and photovoltage is mandatory to optimize the device. An optimized device should exhibit a thin light absorbing layer in order to increase the photocurrent. The effect of blocking layers between the carrier transporting media and the light absorbing layer has to be analyzed in order to compensate the decrease of photovoltage observed for the analyzed samples. In this sense, further increase of the performance of these devices should be expected in the near future. Finally, it is worth noting that the model and the related processes can be easily translated to other all-solid sensitized devices.

Acknowledgements

The authors thank Dr J. Echeberria (CEIT-IK4) for the SEM experiments. This work was supported by the Ministerio de Ciencia e Innovación of Spain under the projects HOPE CSD2007-00007, JES-NANOSOLAR PLE2009-0042, and MAT2007-62982, by Generalitat Valenciana under the project PROMETEO/2009/058 and Basque Regional Government through Etortek Program. R. T-Z. and S.G. acknowledge support from the Program "Ramón y Cajal" of the MICINN.

References

1 V. Gónzalez-Pedro, X. Xu, I. Mora-Seró and J. Bisquert, *ACS Nano*, 2010, **4**, 5783–5790.
2 G. Hodes, *J. Phys. Chem. C*, 2008, **112**, 17778–17787.
3 J. A. Chang, J. H. Rhee, S. H. Im, Y. H. Lee, H.-J. Kim, S. I. Seok, M. K. Nazeeruddin and M. Grätzel, *Nano Lett.*, 2010, **10**, 2609–2612.
4 C. Lévy-Clément, R. Tena-Zaera, M. A. Ryan, A. Katty and G. Hodes, *Adv. Mater.*, 2005, **17**, 1512–1515.
5 P. V. Kamat, *J. Phys. Chem. C*, 2008, **112**, 18737–18753.
6 I. Robel, V. Subramanian, M. Kuno and P. V. Kamat, *J. Am. Chem. Soc.*, 2006, **128**, 2385–2393.
7 H. J. Lee, M. Wang, P. Chen, D. R. Gamelin, S. M. Zakeeruddin, M. Grätzel and M. K. Nazeeruddin, *Nano Lett.*, 2009, **9**, 4221–4227.
8 K. Ernst, M. C. Lux-Steiner and R. Könenkamp, *16th European Photovoltaic Solar Energy Conference*, 2000, 63–66.
9 K. Ernst, A. Belaidi and R. Könenkamp, *Semicond. Sci. Technol.*, 2003, **18**, 475.
10 A. Belaidi, T. Dittrich, D. Kieven, J. Tornow, K. Schwarzburg and M. Lux-Steiner, *Phys. Status Solidi RRL*, 2008, **2**, 172–174.
11 Y. Itzhaik, O. Niitsoo, M. Page and G. Hodes, *J. Phys. Chem. C*, 2009, **113**, 4254–4256.
12 C. Choné and G. Larramona, *French Patent 2899385*, 05, October, 2007.
13 S. Nezu, G. Larramona, C. Chon, A. Jacob, B. Delatouche, D. Péré and C. Moisan, *J. Phys. Chem. C*, 2010, **114**, 6854–6859.
14 S.-J. Moon, Y. Itzhaik, J.-H. Yum, S. M. Zakeeruddin, G. Hodes and M. Grätzel, *J. Phys. Chem. Lett.*, 2010, **1**, 1524–1527.
15 M. Krunks, E. Karber, A. Katerski, K. Otto, I. Oja Acik, T. Dedova and A. Mere, *Sol. Energy Mater. Sol. Cells*, 2010, **94**, 1191–1195.
16 B. O'Regan and M. Gratzel, *Nature*, 1991, **353**, 737–740.
17 W. Yu, L. H. Qu, W. Z. Guo and X. G. Peng, *Chem. Mater.*, 2003, **15**, 2854–2860.
18 R. Tena-Zaera, J. Elias, C. Lévy-Clément, I. Mora-Seró, Y. Luo and J. Bisquert, *Phys. Status Solidi A*, 2008, **205**, 2345–2350.
19 S. Peulon and D. Lincot, *J. Electrochem. Soc.*, 1998, **145**, 864–874.
20 K. R. Taretto, U. Modeling Extremely Thin Absorber Solar Cells for and P. P. R. A. Optimized Design, 12, 573–591, *Progr. Photovolt.: Res. Appl.*, 2004, **12**, 573–591.
21 T. Dittrich, D. Kieven, M. Rusu, A. Belaidi, J. Tornow, K. Schwarzburg and M. Lux-Steiner, *Appl. Phys. Lett.*, 2008, **93**, 053113.
22 I. Mora-Seró, F. Fabregat-Santiago, B. Denier, J. Bisquert, R. Tena-Zaera, J. Elias and C. Lévy-Clément, *Appl. Phys. Lett.*, 2006, **89**, 203117.
23 R. Tena-Zaera, J. Elias, C. Lévy-Clément, C. Bekeny, T. Voss, I. Mora-Seró and J. Bisquert, *J. Phys. Chem. C*, 2008, **112**, 16318–16323.
24 F. Fabregat-Santiago, J. Bisquert, G. Garcia-Belmonte, G. Boschloo and A. Hagfeldt, *Sol. Energy Mater. Sol. Cells*, 2005, **87**, 117–131.
25 J. Elias, R. Tena-Zaera and C. Levy-Clement, *Thin Solid Films*, 2007, **515**, 8553–8557.

26 M. Cocivera, A. Darkowski and B. Love, *J. Electrochem. Soc.*, 1984, **131**, 2514–2517.
27 R. Tena-Zaera, A. Katty, S. Bastide and C. Lévy-Clément, *Chem. Mater.*, 2007, **19**, 1626–1632.
28 B. O'Regan, F. Lenzmann, R. Muis and J. Wienke, *Chem. Mater.*, 2002, **14**, 5023–5029.
29 I. Mora-Seró, S. Giménez, F. Fabregat-Santiago, R. Gómez, Q. Shen, T. Toyoda and J. Bisquert, *Acc. Chem. Res.*, 2009, **42**, 1848–1857.
30 J. Bisquert, *Phys. Chem. Chem. Phys.*, 2000, **2**, 4185–4192.
31 J. Bisquert, *J. Phys. Chem. B*, 2002, **106**, 325–333.
32 J. Bisquert, *Phys. Chem. Chem. Phys.*, 2003, **5**, 5360–5364.
33 R. Tena-Zaera, J. Elias, G. Wang and C. Lévy-Clément, *J. Phys. Chem. C*, 2007, **111**, 16706–16711.
34 F. Fabregat-Santiago, J. Bisquert, L. Cevey, P. Chen, M. Wang, S. M. Zakeeruddin and M. Grätzel, *J. Am. Chem. Soc.*, 2009, **131**, 558–562.
35 J. Bisquert, *J. Phys. Chem. B*, 2002, **106**, 325–333.
36 Y. Y. Proskuryakov, K. Durose, M. K. Al Turkestani, I. Mora-Seró, G. Garcia-Belmonte, F. Fabregat-Santiago, J. Bisquert, V. Barrioz, D. Lamb, S. J. C. Irvine and E. W. Jones, *J. Appl. Phys.*, 2009, **106**, 044507.